Journal of Materials Chemistry A

Accepted Manuscript

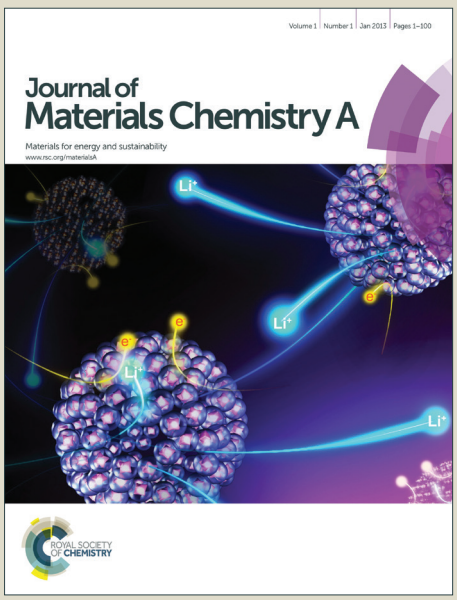

ROYAL SOCIETY OF CHEMISTRY

www.rsc.org/materialsA

Journal of Materials Chemistry

Journal of Materials Chemistry A

Dynamic Article Links ►

Cite this: DOI: 10.1039/c0xx00000x

ARTICLE TYPE

www.rsc.org/xxxxxx

In Situ Growth of Burl-like Nickel Cobalt Sulfide on Carbon Fiber as High-Performance Supercapacitors

Ming Sun, Jinjin Tie, Gao Cheng, Ting Lin, Shaomin Peng, Fangze Deng, Fei Ye, and Lin Yu*

Received (in XXX, XXX) Xth XXXXXXXXX 20XX, Accepted Xth XXXXXXXXX 20XX

DOI: 10.1039/b000000x

Nickel cobalt sulfide ($NiCo_2S_4$), a recently reported novel electrode material, has a higher electric conductivity than that of the $NiCo_2O_4$. We describe a facile one-step route to the development of burl-like $NiCo_2S_4$ on carbon fiber paper/cloth (CFP/CFC) used as electrodes for supercapacitor. The influence of the carbon substrate on the crystal structure and electrochemical performance of the $NiCo_2S_4$ electrodes is evaluated. We obtain pure phase of $NiCo_2S_4$ over CFP substrate, whereas, mixed phase over CFC substrate. Superior pseudocapacitive performance is achieved over $NiCo_2S_4$/CFP with large specific capacitance of 0.83 F cm^{-2} at a high current density of 25 mA cm^{-2}. The capacitance loss is 24.1 % after 5000 cycles at a current density of 20 mA cm^{-2}, displaying good cycle ability and high rate capability.

1 Introduction

Supercapacitors have attracted great interest in the past years because of their prominent properties like high power density, long cycle life, and short charging time[1-3]. Among the factors that affect the performance of supercapacitor, the electrode material is one of the important factors in terms of its morphology, size, dimension, composition and so on. Therefore, various materials like traditional metal oxide, carbon materials, conductive polymer [4] and recently developed metal chalcogenides (CoS, NiS_2, VS_2, $GeSe_2$, etc)[5-7] have been explored extensively aiming to find the ideal candidate with excellent performance and low cost. Thanks to the pioneering work of Prof. Hu and his group in 2010 [8], considerable efforts have been devoted to Nickel cobaltite ($NiCo_2O_4$) prepared by different methods with diverse morphologies. The $NiCo_2O_4$ electrode material is reported to exhibit good electrochemical performance, high electrical conductivity and potential industrialized application[4, 9, 10].

The pace of pursuing excellent electrode material can never stop. We all know that the elements of S and O belong to the same group in the Periodic Table of the Elements, thus the two elements have similar properties. Since $NiCo_2O_4$ has distinguished electrochemical properties, if the element of O is substituted by the element S, then the $NiCo_2S_4$ should also possess similar electrochemical performance. In fact, some binary metal sulfides such as Co sulfide (CoS, CoS_2, Co_9S_8) and Ni sulfide (NiS, Ni_3S_2) have been proposed for a new type of electrode materials[11-17]. Therefore, ternary metal sulfide could have potential application as electrode materials for supercapacitors.

Since 2013, Nickel cobalt sulfide ($NiCo_2S_4$), a new kind of electrode material candidate, has come into being in the region of electrochemical capacitors. Herein, we listed the reported works on $NiCo_2S_4$ in Table 1 as far as we can find. $NiCo_2S_4$ is build around a closely packed array of S^{2-} ions, with Ni^{2+} and Co^{3+} cations occupying the tetrahedral and octahedral sites, respectively[18]. Compared to the $NiCo_2O_4$ material, $NiCo_2S_4$ is reported to have an electric conductivity ~100 times higher than that of $NiCo_2O_4$[19, 20]. Furthermore, $NiCo_2S_4$ with a normal spinel crystal structure possesses more octahedral catalytic active sites of Co^{3+} cations compared to its counterpart with an inverse spinel structure[18]. Compared with binary metal sulfides, $NiCo_2S_4$ can offer richer redox reactions owing to the existence of Co and Ni ions[19, 21]. Based on the above analyses and the practice listed in Table 1, we clear see that the $NiCo_2S_4$ is indeed a kind of outstanding electrode material for supercapacitors.

Table 1 Morphology, synthetic method and specific capacitance of $NiCo_2S_4$ electrode materials

Morphology	Raw materials	Current collector	Specific capacitance	Load mass mg cm^{-2}	Ref
Urchin	$CoCl_2$, $NiCl_2$, Na_2S	-	1065 F g^{-1} (3 A g^{-1})	unknown	20
Nano Sheet/RGO	$Co(NO_3)_2$, $Ni(NO_3)_2$ thiourea	-	1161 F g^{-1} (5 A g^{-1})	unkown	21
Flower, Tube, Cubic, Urchin	$CoCl_2$, $NiCl_2$, Na_2S	-	Tube-1048 F g^{-1} (3 A g^{-1})	4	22
Nanoplate	$CoCl_2$,$Ni(Ac)_2$, Na_2S	-	437 F g^{-1} (1 A g^{-1})	2.4	23
Nanoparticle/GO	$CoCl_2$, $Ni(Ac)_2$, S	-	755 F g^{-1} (4 A g^{-1})	5	24
Nanoparticle	$CoCl_2$, $Ni(Ac)_2$, S	-	770 F g^{-1} (4 A g^{-1})	5	25
Hollow nanoprism	$Co(Ac)_2$, $Ni(Ac)_2$, thioacetamide	-	895 F g^{-1} (1 A g^{-1})	1	26
Nano-Aggregates	$Co(NO_3)_2$, $NiSO_4$, Na_2S	-	592 F g^{-1} (0.5 A g^{-1})	2.5-3.5	27
Nanotube	$CoCl_2$, $NiCl_2$, Na_2S	-	933 F g^{-1} (1 A g^{-1})	4-6	28
Nanotube	$CoCl_2$, $NiCl_2$, Na_2S	Ni foam	738 F g^{-1} (4 A g^{-1})	4.2	29
Nanotube	$CoCl_2$, $NiCl_2$, Na_2S	Ni foam	14.39 F cm^{-2} (5 mA cm^{-2})	6	30
Nanowire	$Co(NO_3)_2$, $Ni(NO_3)_2$, Na_2S	Ni foam	2415 F g^{-1}, 6.0 F cm^{-2}(2.5 mA cm^{-2})	2.5	31
Nanosheet	$Co(Ac)_2$, thioacetamide	Ni foam	5.71 F cm^{-2}(20 mA cm^{-2})	2.1	32
Nanotube	$CoCl_2$, $NiCl_2$, H_2S	Carbon fiber paper	2.86 F cm^{-2} (4 mA cm^{-2}) 0.58 F cm^{-2} (20 mA cm^{-2})	4.3	19
Nanosheet*	$CoCl_2$, $NiCl_2$, thiourea	Carbon cloth	1418 F g^{-1} (5 A g^{-1})	0.8	33

Note: * the material in ref [24], [25] and [33] is $CoNi_2S_4$ instead of $NiCo_2S_4$, we list herein because they are similar material.

Although $NiCo_2S_4$ is gaining the attention of researchers, however, from Table 1, we can see that the obtained results are still limit. First of all, most of the reported were $NiCo_2S_4$ powder instead of integrated electrode [17-25]. The electrodes fabricated by the traditional slurry-coating technique have two disadvantages: one is that the increased "dead surface" leading to the limit of capacitive performance; and the other is that the used binder can decrease the electrical conductivity[34]. Secondly, for the integrated electrodes, the current collector was mainly Ni foam, whereas low-cost carbon materials were rare. Carbon materials usually have large surface area, high porosity and good electric conductivity, and are considered as the backbone for conformal coating of transition metal oxides for supercapacitors[35], thus it is interesting to apply carbon fiber materials as current collector. Thirdly, most of the $NiCo_2S_4$ were prepared by a two-step procedure, which make it complicated and time-consuming to precisely control of the materials. Last, the reported morphology for $NiCo_2S_4$ integrated electrodes were mainly nanotube, nanowire and nanosheet. Because the morphology of material has a substantial influence on the speed of ion transfer and the capacity of charge storage[4], it is desirable to synthesize materials with novel shape.

In order to further exploit the potential of $NiCo_2S_4$ based electrode materials, herein, we proposed a simple one-step solvothermal strategy for the growth of burl-like $NiCo_2S_4$ on two kinds of commercial carbon fiber: carbon fiber paper (CFP) and carbon fiber cloth (CFC). Remarkably, the prepared $NiCo_2S_4$ architectures, especially loaded on CFP, manifests a specific capacitance of 0.83 F cm^{-2} at a high current density of 25 mA cm^{-2} and outstanding cycling stability at high rates. The capacitance of the $NiCo_2S_4$/CFP remained as high as 82.8 % after 5000 cycles at a current density of 20 mA cm^{-2}.

2 Experimental

2.1 Materials and methods

Synthesis of $NiCo_2S_4$ supported on CFP/CFC: All the chemicals were of analytical grade. Commercial CFP or CFC (approximately 1 cm × 4 cm, Shanghai hesen Electronic Co. Ltd.; CFP, Spec: HCP030, 0.30 mm in depth, resistivity: 3 mΩ cm^2 ; CFC, Spec: HCP331, 0.30 mm in depth, resistivity: 3.14 mΩ cm^2 , longitudinal resistance, $<0.1\times10^{-2}\Omega$) were purified under ultrasonic for 15 min in 5M HCl aqueous solution, absolute ethanol and deionized water, respectively. 0.5 mmol of $Co(NO_3)_2\cdot6H_2O$, 0.25 mmol of $Ni(NO_3)_2\cdot6H_2O$, 3 mmol of thioacetamide (TAA) were dissolved into 12 mL of absolute methanol, and then transferred into a 25 mL Teflon-lined stainless steel autoclave. A piece of the pre-treated CFP or CPC was put vertically in the autoclave, heated to 120 °C for 5 h. After the solvothermal process, the products were ultrasonically cleaned with DI water and ethanol, and dried at 60 °C.

2.2 Materials Characterization

The crystal phase of the products was examined by X-ray diffraction diffractometer (XRD, Bruker, D8, Cu Kα, λ=1.5406 Å). The samples were scraped from the carbon fiber carefully for the XRD test. The morphology was characterized by scanning electron microscopy (SEM, Hitachi，S-3400N) and transmission electron microscopy (TEM, Shimadzu, EPMA-1600) equipped with an energy dispersive X-ray spectrometer (EDS). X-ray photoelectron spectroscopy (XPS) was performed on a Thermo ESCALAB 250 instrument equipped with a monochromatic Al Kα (1486.6 eV) X-ray source. The spectra are calibrated using the carbon peak

2.3 Electrochemical Measurements

The cyclic voltammetry (CV) curves and galvanostatic charge-discharge were measured on Autolab PGSTAT302N Electrochemical Workstation in a three-electrode cell containing 2 M KOH aqueous solution as electrolyte at room temperature. The carbon fiber supported electroactive materials (~1 cm^2 in area, loading mass of $NiCo_2S_4$ is *ca*.2.3 mg) serves directly as the working electrode. The counter electrode and the reference electrode were a platinum foil electrode and a saturated calomel electrode (SCE), respectively. The electrochemical impedance spectroscopy (EIS) was tested in a frequency range from 100 kHz to 0.01 Hz at open circuit potential. Areal capacitances are calculated using the equations, $Cs = \frac{I\Delta t}{S\Delta V}$, where *Cs* (F cm^{-2}) is areal capacitance, *I (A)* represented discharge current, *S* (cm^2), ΔV (V), and Δt (s) designate the area of the electrode, potential drop during discharge, and total discharge time, respectively.

3. Results and discussion

3.1 Synthesis and characterization

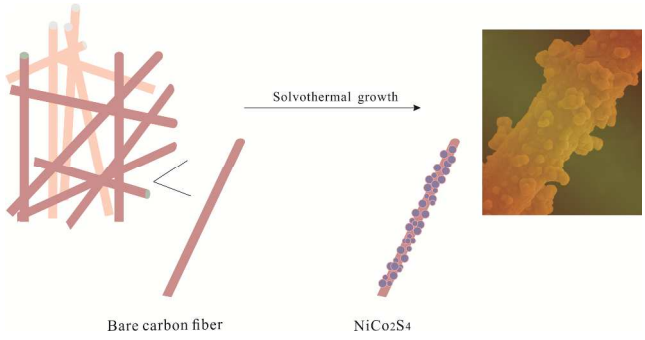

Scheme.1 Schematic illustration of synthetic $NiCo_2S_4$ on CFP/CFC

The synthetic strategy for $NiCo_2S_4$ supported on CFP/CFC is shown in Scheme.1. TAA is used as the sulfur source, it can release sulfide ions in aqueous medium[26]. Burl-like $NiCo_2S_4$ were obtained through the reaction among Co^{2+}, Ni^{2+}, and TAA under solvothermal condition, and many metal sulfides such as MnS, NiS, Ni_3S_4, and $NiCo_2S_4$ have been prepared by similar strategy using TAA as sulfur source[36-38]. Unlike the anion-exchange reaction mechanism widely existed in two-step reaction for synthesis of $NiCo_2S_4$[22, 26, 30, 31], we think that the formation of $NiCo_2S_4$ in our case is through the coprecipitation process as Shimizu et al [37] suggested.

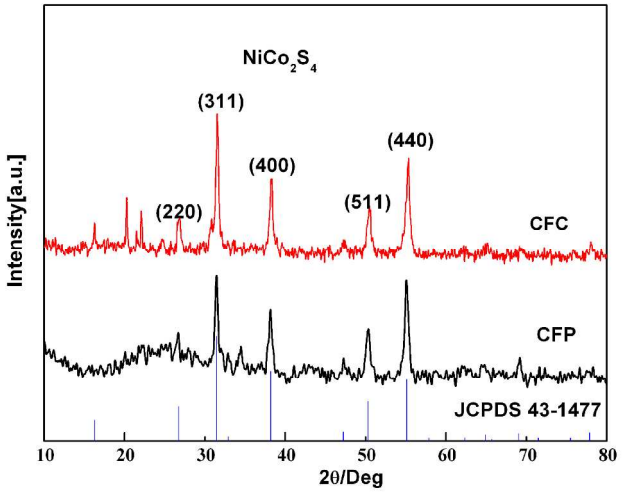

Fig.1 XRD patterns of $NiCo_2S_4$ supported on CFP and CFC

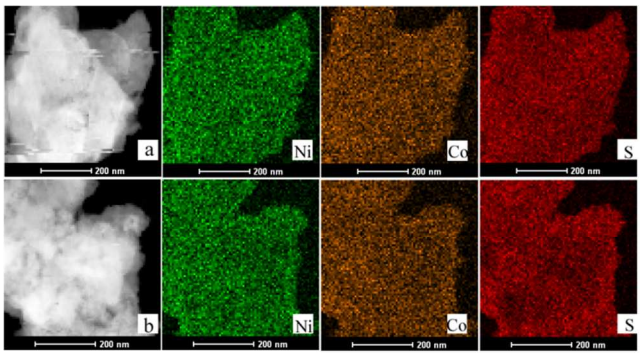

Fig.2 EDX mapping results of (a) $NiCo_2S_4$/ CFP and (b) $NiCo_2S_4$ /CFC

To prove that we have successfully obtained $NiCo_2S_4$, XRD, EDX mapping and XPS characterizations were carried out. Fig. 1 shows the XRD patterns of the $NiCo_2S_4$ samples loaded on CFP and CFC substrate. For the two samples, they both show diffraction peaks at 26.8 °, 31.5 °, 38.1 °, 50.4 ° and 55.2 ° corresponding to the respective (220), (311), (400), (511) and (440) planes of the cubic type $NiCo_2S_4$ (JCPDS# 43-1477). However, for the CFC loaded sample, there are two extra peaks located at around 20 ° and 22 °. These impurity peaks can be assigned to the S (JCPDS#24-1251) formed by the decomposition of TAA. To better understand the presence of impurity, we use SEM-EDX to examine the difference between CFP and CFC substrate. As shown in Supporting Information Fig.S(1-2), the CFP is mainly composed by C (~99 *wt* %) and O (~1 *wt*%). However, besides C and O element, the CFC contains other impurities such as Na (~0.1 *wt*%), Si (~0.1 *wt*%), and P(~0.3 *wt*%). Such unexpected impurities in CFC substrate might lead to the presence of S in $NiCo_2S_4$ under solvothermal conditions. The difference in the phase structure demonstrate that the substrate can not only influence the final morphology of active materials under solvothermal condition[39], but also can affect the purity of crystal phase. The mapping images (Fig.2) of Ni, Co, and S show uniform and continuous dispersion throughout the carbon fiber, indicating that homogeneous $NiCo_2S_4$ materials were covered on the carbon fiber substrate. The $NiCo_2S_4$ loaded on CFP and CFC show similar XPS spectra as displayed in Fig.3. As shown in Fig.3a, the energy difference between Ni $2p_{3/2}$ (853 eV) and Ni $2p_{1/2}$ (870 eV) indicate the existence of both divalent and trivalent states of Ni[19, 23]. As regards for the Co 2p spectrum, two strong peaks at 779.0 eV for Co $2p_{3/2}$ and 794.0 eV for Co $2p_{1/2}$ can be found, suggesting the coexistence of Co (Ⅲ) and Co(Ⅱ) [19, 23].[19, 23] As for the S 2p spectrum, it can be divided into two main peaks located at around 162.0 and 163.2 eV and one shake-up satellite at about 169.0 eV. The component at 163.2 eV is characteristics of metal-sulphur bonds, while the peak at 162.0 can be assigned to the sulphur ion in low coordination on the surface[20].

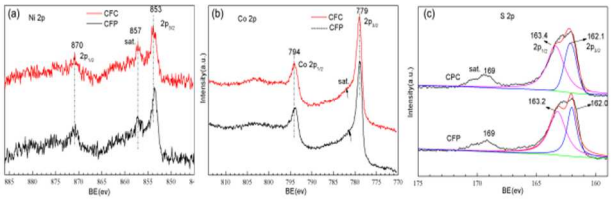

Fig.3 XPS spectra of (a) Co 2p, (b) Ni 2p, and (c) S 2p for the $NiCo_2S_4$.

Cite this: DOI: 10.1039/c0xx00000x

www.rsc.org/xxxxxx

ARTICLE TYPE

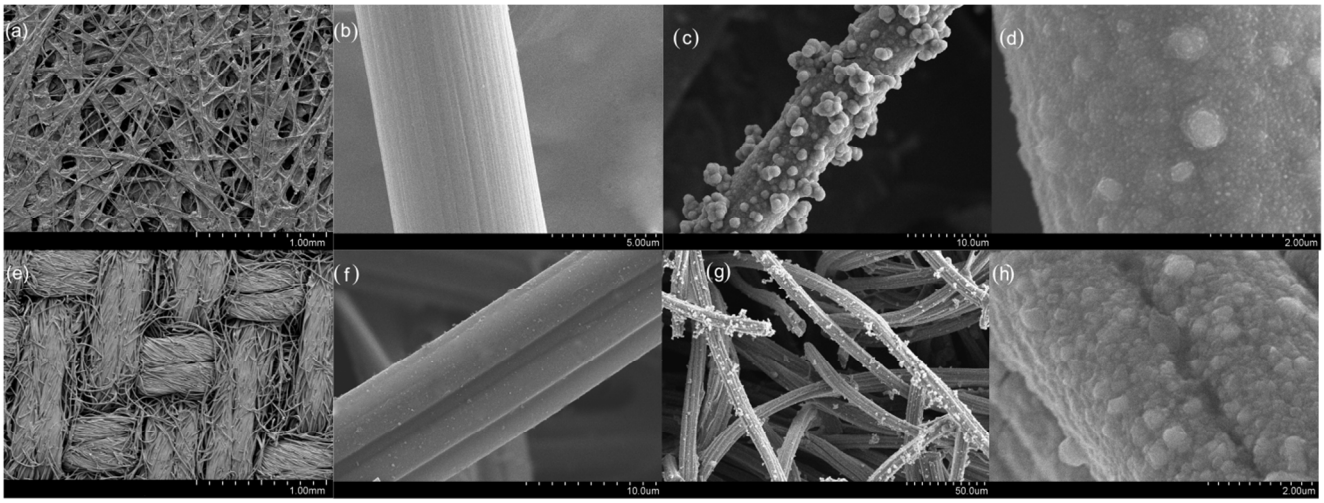

Fig.4 SEM images of (a-b) bare CFP, (c-d) $NiCo_2S_4$/CFP, (e-f) bare CFC, and (g-h) $NiCo_2S_4$ / CFC

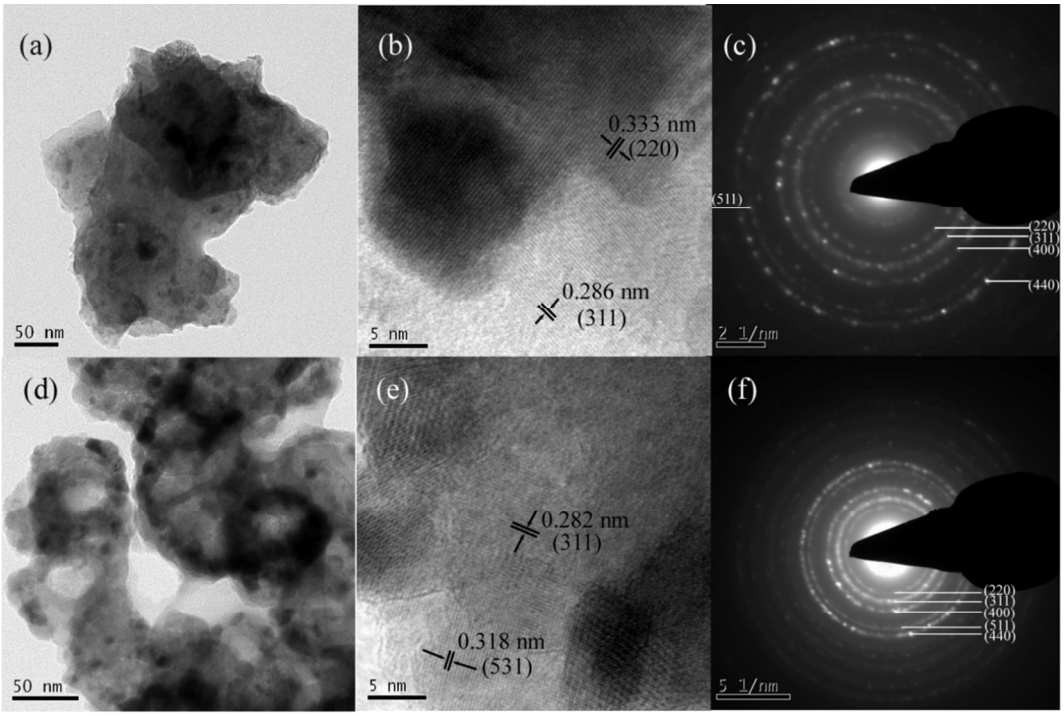

Fig. 5TEM, HRTEM images and SAED patterns of (a-c) $NiCo_2S_4$/CFP, and (d-f) $NiCo_2S_4$/CFC

SEM and TEM tests provide further insights into the morphologies and detailed geometrical structures of the $NiCo_2S_4$ materials. The low magnification image of CFP is displayed in Fig.2(a), the carbon fiber interconnects with each other formed web-like structure. If examine carefully, we can see that the carbon fiber in CFP has very smooth surface (Fig.2b). However, for the CFC, it shows the typical morphology of carbon cloth with crossed carbon fiber, and the surface of its carbon fiber is

dotted with tiny flakes (Fig.2(e-f)). After solvothermal process with the source chemicals, as shown in Fig.4 (c-d), a large quantity of burl-like $NiCo_2S_4$ have grown on the surface of the carbon fiber substrate. Similar phenomena can be observed over the CFC supported $NiCo_2S_4$ material (Fig. 4 (g-h)) and the surface of CFC has been dotted with $NiCo_2S_4$ humps. The TEM, HRTEM and corresponding SAED patterns of $NiCo_2S_4$ scraped down from CFP and CFC are displayed in Fig.5 (a-c) and Fig.5 (d-f), respectively. As for $NiCo_2S_4$ supported on CFP, we can see from Fig. 5a that the $NiCo_2S_4$ burls are actually composed of different size of nanoflakes. Based on the HRTEM image (Fig. 5b), the lattice spacing of 0.286 nm and 0.333 nm corresponds to the (311) and (220) crystal planes of $NiCo_2S_4$. The SAED pattern (Fig.5c) demonstrates a polycrystalline structure, and the diffraction rings can be indexed to the (220), (311), (400), (511) and (440) planes of $NiCo_2S_4$. As for $NiCo_2S_4$ supported on CFC, it is also constructed by small nanoflakes (Fig.5d). Meanwhile, its lattice fringes shown in Fig. 5e can be indexed to the (311) and (531) crystal planes of the $NiCo_2S_4$. The SAED pattern in Fig. 5f confirms the polycrystalline nature of the material.

3.2 Electrochemical characterization

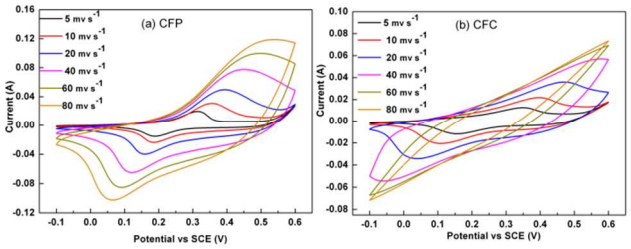

Fig.6 The CV curves of the (a) $NiCo_2S_4$/CFP electrode and (b) $NiCo_2S_4$/CFC electrode at different scan rates of 5, 10, 20, 40, 60 and 80 mV s^{-1}

The electrochemical properties of the prepared $NiCo_2S_4$ materials were investigated in the three-electrode measurements with 2 M KOH as the electrolyte. The cyclic voltammetry (CV) measurements under different scan rate are representing in Fig. 6. The cyclic voltammograms of $NiCo_2S_4$ grown over CFP substrate display a distinct pair of redox peaks during the positive and negative sweeps (Fig. 6a). The shape of the CV curves reveals the pseudocapacitive characteristics of the $NiCo_2S_4$ electrode, which agrees well with the previous reports [24, 25, 32]. The redox peaks are caused by the reversible redox reaction of $NiCo_2S_4$ in alkaline electrolyte according to the following equation[19, 30, 32]:

$$NiCo_2S_4 + 2OH^{-1} \rightarrow NiS_{4-2x}OH + 2CoS_xOH + 2e^-$$

Compared with the CV curves of the $NiCo_2S_4$/CFP, as observed from Fig.5b, the $NiCo_2S_4$/CFC behaves a relatively less obvious pair of redox peaks. Especially, under high scan rate (>40 mV s^{-1}), the redox peaks almost disappear, and this indicates that the polarization of the $NiCo_2S_4$/CFC electrode is more serious than that of $NiCo_2S_4$/CFP.

To compare the influence of substrate on capacitance, the CV cures of $NiCo_2S_4$/CFP and $NiCo_2S_4$/CFC under the same scan rate of 20 mV s^{-1} are shown in Supporting Information Fig. S2. Form Fig.S 2, we can clear observe that the variation in redox peaks position for the two samples, and this phenomena is due to the difference in electrode polarization behaviours[32]. As the specific capacitance is proportional to the area of the CV curve, apparently, $NiCo_2S_4$/CFP shows bigger CV curve area than that of the $NiCo_2S_4$/CFC, indicating that $NiCo_2S_4$/CFP has higher capacitance and better electrochemical activity. Based on the CV analysis, CFP is more suitable to be used as current collector than CFC.

Cite this: DOI: 10.1039/c0xx00000x

www.rsc.org/xxxxxx

ARTICLE TYPE

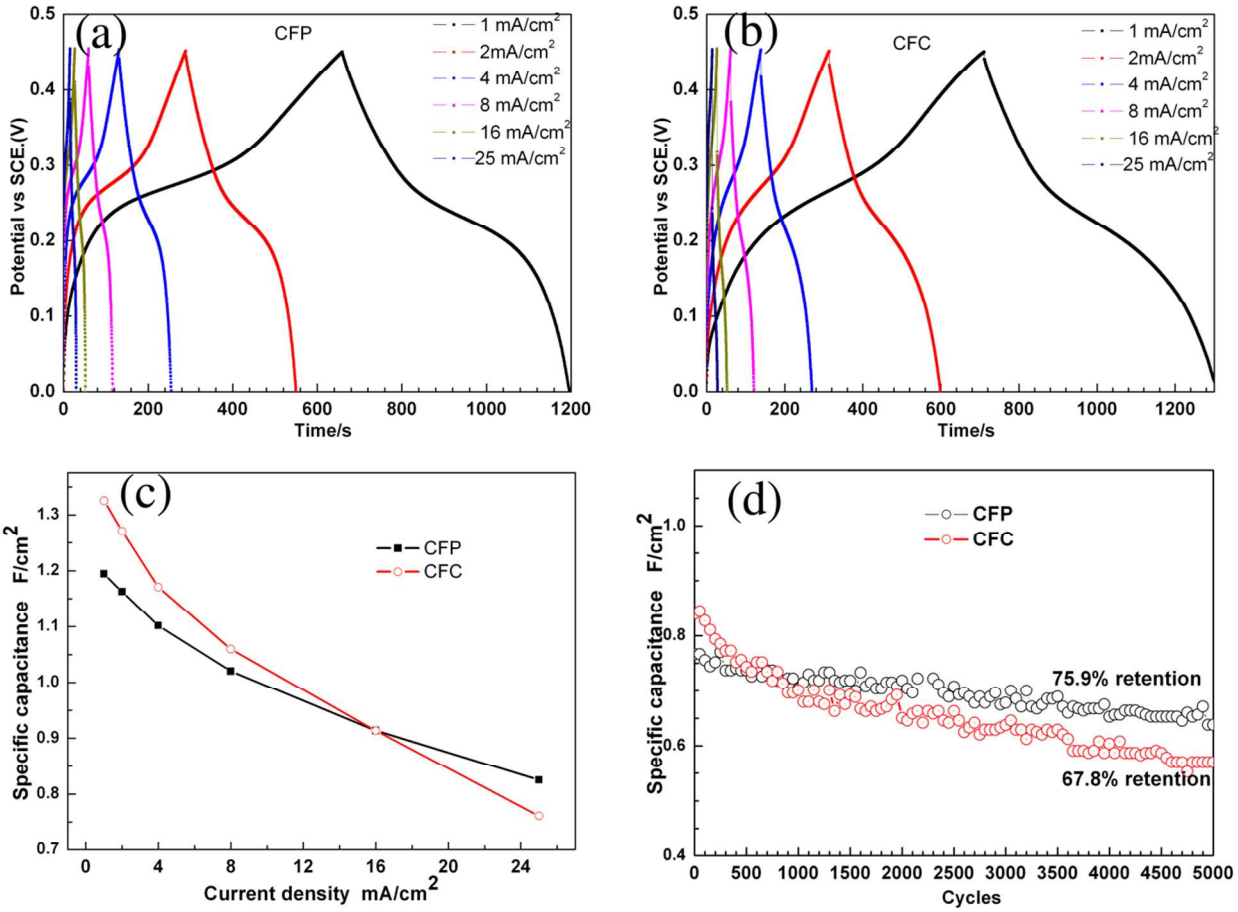

Fig.7 Galvanostatic current charge-discharge curves of (a) $NiCo_2S_4$/CFP electrode and (b) $NiCo_2S_4$/CFC electrode at different current density; (c) the specific capacitance as a function of current density of the $NiCo_2S_4$/CFP and $NiCo_2S_4$/CFC electrode; (d) the cycling performance at constant current density of 20 mA cm^{-2} of the two electrodes.

To further evaluate the capacitive performance of the $NiCo_2S_4$/CFP and $NiCo_2S_4$/CFC electrodes, we carried out galvanostatic charge-discharge test, and the results are shown in Fig. 7(a-b). The comparison of galvanostatic charge-discharge curves for the two samples at a constant current density of 25 mA cm^{-2} is given in Fig.S 3(Supporting Information). The plateaus in the charge/discharge curves imply the existence of Faradaic process which is related with the Ni ions and Co ions [19, 30], and this result is consistent with the CV analysis. Obviously, the charge-discharge curves of $NiCo_2S_4$/CFP are more symmetric at high current density (for example, 16 and 25 mA cm^{-2}), implying that the $NiCo_2S_4$/CFP electrode has higher charge-discharge coulombic efficiency and lower polarization [34, 40]. The specific capacitances of the two $NiCo_2S_4$ products are present in Fig.7c as function of current density. Specifically, the specific capacitance of the $NiCo_2S_4$/CFP is 1.19, 1.16, 1.10, 1.02, 0.91 and 0.83 F cm^{-2} at the current density of 1, 2, 4, 8, 16 and 25 mA cm^{-2}, respectively. In contrast, under the same series of current density, the specific capacitance of the $NiCo_2S_4$/CFC is 1.33, 1.27, 1.17, 1.06, 0.91 and 0.76 F cm^{-2}. At lower current density, ions can penetrate into the inner-structure of electrode material and make full use of the active material, thus leading to a relatively higher specific capacitance. At higher current density, on the contrary, only the outer surface of electrodes can be effective utilized, thus resulting in a relatively lower specific capacitance[32, 41]. Therefore, with the current density rising, the specific capacitance is decreasing accordingly. Despite that our prepared $NiCo_2S_4$/CFP do not show excellent specific capacitance as the reported $NiCo_2S_4$ [30-32], however, the $NiCo_2S_4$/CFP dose exhibits superior specific capacitance than those $NiCo_2S_4$ [19, 23, 26] and better

electrochemical activity than $NiCo_2O_4$ supported on carbon fiber [42-45]. Furthermore, for $NiCo_2S_4$/CFP, there is around 70 % initial capacitance retention as the current density increases from 1 mA cm^{-2} to 25 mA cm^{-2}, and the high-rate capability is better than that of $NiCo_2S_4$/CFC with only 57% initial capacitance retention. This relatively good rate capability is critical for its potential application.

The long-term stability was tested by galvanostatic charge-discharge cycling at a current density of 20 mA cm^{-2} (Fig. 7d). For $NiCo_2S_4$/CFP electrode, the capacitance decreased slowly, and the total capacitance loss is 24.1 % after 5000 cycles. To the best of our knowledge, the cycling performance of the $NiCo_2S_4$/CFP electrode is worse than that of reported $NiCo_2S_4$ [19, 20, 30, 32], but superior to those previously reported values [21-24]. In comparison, the capacitance loss for $NiCo_2S_4$/CFC electrode is ~32.2 %. The charge-discharge efficiency, namely Coulombic efficiency, is estimated according to the following equation: $\eta = t_d / t_c \times 100\%$, where t_c and t_d are the charge and discharge intervals, respectively. The two electrode materials exhibited a higher charge-discharge efficiency of ~99% during the entire test. From the electrochemical characterization, the $NiCo_2S_4$/CFP electrode exhibits superior electrochemical performance with both higher capacitance and better cycling stability than that of $NiCo_2S_4$/CFC. Based on the structure and morphology characterization, we know that the two $NiCo_2S_4$ have similar morphology but different body composition. $NiCo_2S_4$ supported over CFC is not pure but with impurity, and this might the main reason for such variation in electrochemical performance.

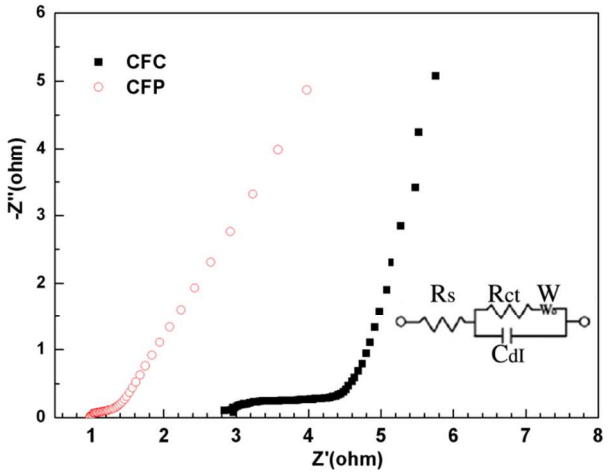

Fig.8 Nyquist plots of the EIS of the $NiCo_2S_4$/CFP and $NiCo_2S_4$/CFC electrode at bias potential of 0.35 V and the equivalent circuit of diagram.

To gain further insight into the transport kinetics of the electrochemical behaviours, we resorted to electrochemical impedance spectroscopy (EIS) carried out at open circuit potential in the frequency range between 0.01 Hz and 100 kHz. Fig. 8 shows the EIS of the $NiCo_2S_4$/CFP and $NiCo_2S_4$/CFC electrodes and the equivalent circuit is present inset. Where, the equivalent circuit includes the following parameters: equivalent series resistance (R_s), charge-transfer resistance (R_{ct}), double-layer capacitance (C_{dl}), pseudocapacitance (C_{ps}) and Warburg behaviour (W). The R_s for the $NiCo_2S_4$/CFP and is *ca*. 0.98 Ω, which is much smaller than that of $NiCo_2S_4$/CFC (2.83 Ω). The smaller R_s value of $NiCo_2S_4$/CFP indicates that the interfacial contact between $NiCo_2S_4$ deposits and carbon fiber paper are consistent. Furthermore, the $NiCo_2S_4$/CFP electrode displays even smaller diameter of the semicircle in the impedance spectrum than that of $NiCo_2S_4$/CFC electrode, and this indicates that $NiCo_2S_4$/CFP has relatively lower charge-transfer resistance. Such difference in EIS of the two samples might is caused by the impurity of the $NiCo_2S_4$/CFC. In general, the EIS results clearly demonstrate that the $NiCo_2S_4$/CFP exhibits favourable charge-transfer kinetics and fast electron transport compared to $NiCo_2S_4$/CFC, and thus further proving that $NiCo_2S_4$/CFP electrode has superior electrochemical performance compared to its counterpart.

Conclusions

In summary, we have prepared two kinds of $NiCo_2S_4$ electrodes supported on carbon fiber paper and carbon fiber cloth respectively using a facile one-step solvothermal method. Although they both belong to carbon fiber materials, however, the substrates do matter in terms of the supported $NiCo_2S_4$ purity and activity! The $NiCo_2S_4$/CFP exhibited favourable charge-transfer kinetics and fast electron transport compared to $NiCo_2S_4$/CFC, and thus showing superior electrochemical performance than its counterpart. The self-supported hybrid $NiCo_2S_4$/CFP electrode showed high specific capacitance of 1.19 and 0.83 F cm^{-2} at current densities of 1 and 25 mA cm^{-2}, respectively, and exhibited desirable cycling stability as well as high rate capability. Considering the facile and cost-effective synthesis route and relatively high performance, the $NiCo_2S_4$/CFP might hold great promise as an active electrode for electrochemical supercapacitor.

Acknowledgments

This work was financially supported by the National Natural Science Foundation of China (21306026), Natural Science Foundation of Guangdong Province (S2012010009680), the Foundation of Higher Education of Guangdong Province (cgzhzd1104, 2013CXZDA016), and Foundation for Distinguished Young Talents in Higher Education of Guangdong (2013LYM0024).

Notes and references

[a] *School of Chemical Engineering and Light Industry, Guangdong University of Technology, Guangzhou 510006, P. R.China. Fax: 86 20 3932 2237;*
[*] *E-mail: Gych@gdut.edu.cn*

† Electronic Supplementary Information (ESI) available: [details of any supplementary information available should be included here]. See DOI: 10.1039/b000000x/

1. P. Simon and Y. Gogotsi, *Nat. Mater.*, 2008, **7**, 845-854.
2. G. Wang, L. Zhang and J. Zhang, *Chem.Soc. Rev.*, 2012, **41**, 797-828.
3. P. J. Hall, M. Mirzaeian, S. I. Fletcher, F. B. Sillars, A. J. R. Rennie, G. O. Shitta-Bey, G. Wilson, A. Cruden and R. Carter, *Energy Environ. Sci.*, 2010, **3**, 1238.

4. Z. Wu, Y. Zhu and X. Ji, *J. Mater. Chem. A*, 2014, **2**, 14759-14772.
5. M. R. Gao, Y. F. Xu, J. Jiang and S. H. Yu, *Chem. Soc. Rev.*, 2013, **42**, 2986-3017.
6. X. Wang, B. Liu, Q. Wang, W. Song, X. Hou, D. Chen, Y. B. Cheng and G. Shen, *Adv. Mater.*, 2013, **25**, 1479-1486.
7. J. Feng, X. Sun, C. Wu, L. Peng, C. Lin, S. Hu, J. Yang and Y. Xie, *J. Am. Chem. Soc.*, 2011, **133**, 17832-17838.
8. T. Y. Wei, C. H. Chen, H. C. Chien, S. Y. Lu and C. C. Hu, *Adv. Mater.*, 2010, **22**, 347-351.
9. G. Zhang and X. W. Lou, *Adv. Mater.*, 2013, **25**, 976-979.
10. G. Zhang, B. Y. Xia, X. Wang and X. W. David Lou, *Adv. Mater.*, 2014, **26**, 2408-2412.
11. J. Xu, Q. Wang, X. Wang, Q. Xiang, B. Liang, D. Chen and G. Shen, *ACS Nano*, 2013, **7**, 5453-5462.
12. W. Wei, L. Mi, Y. Gao, Z. Zheng, W. Chen and X. Guan, *Chem. Mater.*, 2014, **26**, 3418-3426.
13. J. Pu, Z. Wang, K. Wu, N. Yu and E. Sheng, *Phys. Chem. Chem. Phys.*, 2014, **16**, 785-791.
14. S. Amaresh, K. Karthikeyan, I. C. Jang and Y. S. Lee, *J. Mater. Chem. A*, 2014, **2**, 11099-11106.
15. S. Peng, L. Li, H. Tan, R. Cai, W. Shi, C. Li, S. G. Mhaisalkar, M. Srinivasan, S. Ramakrishna and Q. Yan, *Adv. Funct. Mater.*, 2014, **24**, 2155-2162.
16. Z. Xing, Q. Chu, X. Ren, C. Ge, A. H. Qusti, A. M. Asiri, A. O. Al-Youbi and X. Sun, *J. Power Sources*, 2014, **245**, 463-467.
17. Q. Wang, L. Jiao, H. Du, J. Yang, Q. Huan, W. Peng, Y. Si, Y. Wang and H. Yuan, *CrystEngComm*, 2011, **13**, 6960-6963.
18. Z. Zhang, X. Wang, G. Cui, A. Zhang, X. Zhou, H. Xu and L. Gu, *Nanoscale*, 2014, **6**, 3540-3544.
19. J. Xiao, L. Wan, S. Yang, F. Xiao and S. Wang, *Nano Lett.*, 2014, **14**, 831-838.
20. H. Chen, J. Jiang, L. Zhang, H. Wan, T. Qi and D. Xia, *Nanoscale*, 2013, **5**, 8879-8883.
21. S. Peng, L. Li, C. Li, H. Tan, R. Cai, H. Yu, S. Mhaisalkar, M. Srinivasan, S. Ramakrishna and Q. Yan, *Chem Commun* 2013, **49**, 10178-10180.
22. Y. Zhang, M. Ma, J. Yang, C. Sun, H. Su, W. Huang and X. Dong, *Nanoscale*, 2014, **6**, 9824-9830.
23. J. Pu, F. Cui, S. Chu, T. Wang, E. Sheng and Z. Wang, *ACS Sustainable Chemistry & Engineering*, 2014, **2**, 809-815.
24. W. Du, Z. Wang, Z. Zhu, S. Hu, X. Zhu, Y. Shi, H. Pang and X. Qian, *J. Mater. Chem. A*, 2014, **2**, 9613-9619.
25. W. Du, Z. Zhu, Y. Wang, J. Liu, W. Yang, X. Qian and H. Pang, *RSC Advances*, 2014, **4**, 6998-7002.
26. L. Yu, L. Zhang, H. B. Wu and X. W. Lou, *Angew. Chem. Int. Ed.*, 2014, **53**, 3711-3714.
27. L. Liu, *Nanoscale*, 2013, **5**, 11615-11619.
28. H. Wan, J. Jiang, J. Yu, K. Xu, L. Miao, L. Zhang, H. Chen and Y. Ruan, *CrystEngComm*, 2013, **15**, 7649-7651.
29. J. Pu, T. Wang, H. Wang, Y. Tong, C. Lu, W. Kong and Z. Wang, *ChemPlusChem*, 2014, **79**, 577-583.
30. H. Chen, J. Jiang, L. Zhang, D. Xia, Y. Zhao, D. Guo, T. Qi and H. Wan, *J. Power Sources*, 2014, **254**, 249-257.
31. Y. Li, L. Cao, L. Qiao, M. Zhou, Y. Yang, P. Xiao and Y. Zhang, *J. Mater. Chem. A*, 2014, **2**, 6540-6548.
32. L. Mei, T. Yang, C. Xu, M. Zhang, L. Chen, Q. Li and T. Wang, *Nano Energy*, 2014, **3**, 36-45.
33. W. Chen, C. Xia and H. N. Alshareef, *ACS Nano*, 2014, **8**, 9531-9541.
34. C. Yuan, J. Li, L. Hou, X. Zhang, L. Shen and X. W. D. Lou, *Adv. Funct. Mater.*, 2012, **22**, 4592-4597.
35. F. Deng, L. Yu, G. Cheng, T. Lin, M. Sun, F. Ye and Y. Li, *J. Power Sources*, 2014, **251**, 202-207.
36. Y. Zhang, H. Wang, B. Wang, H. Yan and M. Yoshimura, *J. Cryst. Growth*, 2002, **243**, 214-217.
37. Y. Shimizu and T. Yano, *Chem. Lett.*, 2001, 1028-1029.
38. J. Grau and M. Akinc, *J. Am. Ceram. Soc.*, 1996, **79**, 1073-1082.
39. R. B. Rakhi, W. Chen, D. Cha and H. N. Alshareef, *Nano Lett.*, 2012, **12**, 2559-2567.
40. L. Yang, S. Cheng, Y. Ding, X. Zhu, Z. L. Wang and M. Liu, *Nano Lett.*, 2012, **12**, 321-325.
41. H. Li, M. Yu, F. Wang, P. Liu, Y. Liang, J. Xiao, C. X. Wang, Y. Tong and G. Yang, *Nat Commun*, 2013, **4**, 1894.
42. H. Wang, Z.Hu, Y. Chang, Y.Chen, H.Wu, Z. Zhang and Y.Yang, *J. Mater. Chem.*, 2011, **21**, 10504-10511.
43. H. Wang, Q. Gao and L. Jiang, *Small*, 2011, **7**, 2454-2459.
44. L. Huang, D. Chen, Y. Ding, S. Feng, Z. L. Wang and M. Liu, *Nano Lett.*, 2013, **13**, 3135-3139.
45. N. Padmanathan and S. Selladurai, *RSC Advances*, 2014, **4**, 8341-8349.

table of contents entry

$NiCo_2S_4$/CFP displayed good cycle ability and high rate capability with capacitance loss of 24.1 % after 5000 cycles.